Chinese Chemical Letters 34 (2023) 108127

Contents lists available at ScienceDirect

Chinese Chemical Letters

journal homepage: www.elsevier.com/locate/cclet

An organic-inorganic hybrid thermochromic ferroelastic with multi-channel switches

Yipiao Zeng[1], Junchao Liu[1], Lin Zhou[1], Xin Deng, Wenli Yang, Xin Yan, Yanling Luo, Xuan Zhu, Xiaoyun Huang, Xianjiang Song*, Yuanyuan Tang*

Ordered Matter Science Research Center and School of Chemistry and Chemical Engineering, Nanchang University, Nanchang 330031, China

ARTICLE INFO

Article history:
Received 24 September 2022
Revised 11 November 2022
Accepted 30 December 2022
Available online 1 January 2023

Keywords:
Organic-inorganic hybrid compounds
Ferroelastic domains
Thermochromism
Multi-channel switches
Bistability

ABSTRACT

Multifunctional switchable materials are attracting tremendous interest because of their great application potential in signal processing, information encryption, and smart devices. Here, we reported an organic-inorganic hybrid thermochromic ferroelastic crystal, [TMIm][$CuCl_4$] (TMIm = 1,1,3,3-tetramethylimidazolidinium), which undergoes two reversible phase transitions at 333 K and 419 K, respectively. Intriguingly, these three phases experience a remarkable ferroelastic-paraelastic-ferroelastic (2/*m*-*mmm*-2/*m*) transition, which remains relatively unexplored in ferroelastics. Moreover, the ferroelastic domains can be simultaneously switched under temperature and stress stimuli. Meanwhile, [TMIm][$CuCl_4$] exhibits thermochromic phenomenon, endowing it with extra spectral encryption possibilities during information processing. Combined with dielectric switching behavior, [TMIm][$CuCl_4$] are promising for practical applications in memory devices, next-generation sensors, and encryption technology.

Multi-channel information processing and encryption capabilities play an important role among a variety of smart device materials for satisfying the development needs of the mega data era [1–3]. Switching materials, which can be switched in two relatively stable states with different physical properties under external stimulation (such as electrical, magnetic, thermal, optical, and mechanical fields), are widely utilized in signal processing, intelligent devices, sensors, and so on [4–17]. Bistability with switching on/off in switching materials is beneficial to data storage and encryption technology [18]. Bistable materials with multiple physical channels can not only enhance the strength of information encryption but also expand its practical application range, which would provide more opportunities and freedom to design devices [19,20].

Organic-inorganic hybrid compounds are considered prospective candidates for switching materials due to their inherent structural flexibility, easy processability, low acoustical, and lightweight, with great promise for next-generation ductile and wearable devices [21–30]. The coexistence and/or coupling of dielectric-ferroelectric, luminescence-ferroelectric, and ferromagnetic-ferroelectric have been reported in organic-inorganic hybrid systems, such as $MPSnBr_3$ (MP = methylphosphonium), tetramethylphosphonium tetrachloroferrate(III) ($[(CH_3)_4P][FeCl_4]$, $[3,3\text{-difluorocyclobutylammonium}]_2CrCl_4$ [31–41]. However, switching materials which exhibit bistability with three or more physical channels simultaneously are still scarce. In this context, combining multiple physical channels into a single material remains a big challenge.

In recent years, the design of multifunctional switching materials was injected new vitality due to "Ferroelectrochemistry" proposed by Xiong *et al.* [42,43]. Inspired by "Ferroelectrochemistry", we successfully obtained an organic-inorganic hybrid thermochromic ferroelastic crystal with multi-channel switches, [TMIm][$CuCl_4$] (TMIm = 1,1,3,3-tetramethylimidazolidinium), which undergoes two reversible phase transitions at 333 K (T_{c1}) and 419 K (T_{c2}), respectively. Noteworthily, it exhibits switchable bistability in three channels of dielectric, thermochromic, and ferroelastic properties simultaneously. [TMIm][$CuCl_4$] can be rapidly switched between a low dielectric state and a high dielectric state, which makes it a promising candidate for dielectric switching material [44–46]. More importantly, the distortion of the [$CuCl_4$] tetrahedron under the thermal stimuli produces a fascinating thermochromic phenomenon, which has great potential applications in devices such as smart windows, visual thermometers, and temperature sensors [47–49]. Intriguingly, [TMIm][$CuCl_4$] undergoes a unique ferroelastic-paraelastic-

* Corresponding authors.
E-mail addresses: songxj@ncu.edu.cn (X. Song), tangyuanyuan@ncu.edu.cn (Y. Tang).
[1] These authors contributed equally to this work.

https://doi.org/10.1016/j.cclet.2022.108127
1001-8417/

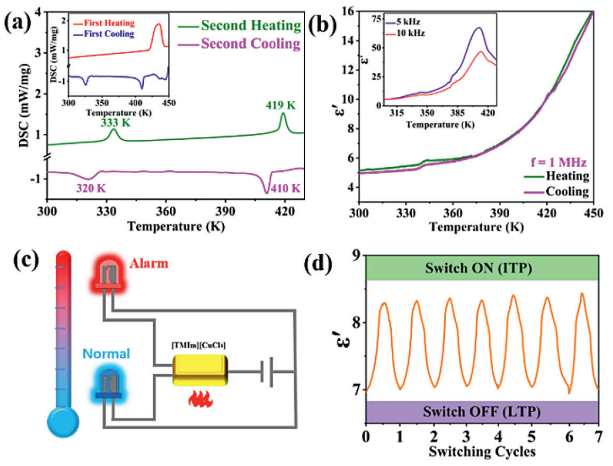

Fig. 1. (a) The DSC curve of [TMIm][$CuCl_4$] measured in second heating-cooling cycle. Inset: the DSC curve of [TMIm][$CuCl_4$] measured in first heating-cooling cycle. (b) The temperature-dependence ε' of [TMIm][$CuCl_4$] at 1 MHz in the heating and cooling cycle. Inset: the ε' of [TMIm][$CuCl_4$] at 5 kHz and 10 kHz in the heating. (c) Working concept diagram of smart device in [TMIm][$CuCl_4$]. (d) The switching cycles of the dielectric measurement for [TMIm][$CuCl_4$].

ferroelastic phase transition, which is very rare among the previously reported types of ferroelastic transitions. Furthermore, ferroelastic domains can be rapidly switched by thermal stimulation and external stress in [TMIm][$CuCl_4$]. Due to multi-channel physical switches, [TMIm][$CuCl_4$] would be of great significance for multiplex information processing and encryption in smart devices, information storage, *etc*., and has potential application prospects in the field of modern information. This work paves the way for the development of new multifunctional switching materials.

Differential scanning calorimetry (DSC) is the primary way to test whether the phase transition behavior occurs. In the first cycle of heating and cooling, [TMIm][$CuCl_4$] has an endothermic peak on the heating curve and a corresponding exothermic peak on the cooling curve (inset of Fig. 1a). Notably, a new exothermic peak appeared at 325 K during cooling. In subsequent measurements, two pairs of thermal anomaly peaks appeared at 333/320 K (T_{c1}) and 419/410 K (T_{c2}) as shown in Fig. 1a, accompanied by wide thermal hysteresis, 13 and 9 K, respectively, indicating that both phase transitions are first-order ones [50]. For convenience, the phase with a temperature higher than T_{c2} is denoted as the high-temperature phase (HTP), that between T_{c1} and T_{c2} as the intermediate-temperature phase (ITP), and that below T_{c1} is recorded as the low-temperature phase (LTP). From the DSC data, entropy changes ΔS_1 and ΔS_2 were calculated to be 8.89 and 7.45 J mol^{-1} K^{-1}, respectively. In accordance with the Boltzmann equation $\Delta S = R\ln(N)$, the N values for two phase transitions are estimated to be about 3.14 and 2.23, respectively, proving that both phase transitions are order-disorder ones [51].

To further verify the phase transition behavior, we measured the variable-temperature dielectric constant of [TMIm][$CuCl_4$] in the temperature range of 300–450 K. As shown in Fig. 1b, the real part ε' exhibits a pair of distinct step-like dielectric anomalies between LTP and ITP at a frequency of 1 MHz, with a gradual increase in ε' value around T_{c1}. Then the second dielectric anomaly was observed at about T_{c2}, and the corresponding more obvious dielectric peaks could be seen at 5 kHz and 10 kHz (inset of Fig. 1b). Hence, the existence of phase transitions is proved by two pairs of obvious dielectric anomalies, which are in good agreement with the thermal analysis results.

As shown in Fig. 1d, in the vicinity of T_{c1}, the region with a relatively low ε' value was denoted as "OFF" (LTP), and the region with a relatively high ε' value was denoted as "ON" (ITP). The rapid switching of the dielectric signal between temperature-controlled high and low dielectric states reveals that [TMIm][$CuCl_4$] possesses good dielectric switching properties. Furthermore, good reversibility and sustainability are exhibited in long-term measurements, indicating that [TMIm][$CuCl_4$] has great potential for smart device applications (Fig. 1c) [52,53].

To deeply study the mechanism of microstructural change, the single crystal of [TMIm][$CuCl_4$] was measured with variable-temperature X-ray diffraction. In the initial heating stage, [TMIm][$CuCl_4$] crystallizes in orthorhombic space group $Pna2_1$ (point group $mm2$) at 298 K and 373 K, respectively (Table S1 and Fig. S4 in Supporting information). When the temperature exceeds T_{c2}, [TMIm][$CuCl_4$] crystallizes in monoclinic space group $C2/c$ (point group $2/m$) with unit cell parameters of a =14.4227(18) Å, b = 7.8394(10) Å, c = 12.5370(19) Å, β = 92.499°, V = 1416.84(3) $Å^3$, Z = 4. When the temperature returns to 298 K again (RTP), [TMIm][$CuCl_4$] crystallizes in the monoclinic space group $C2/c$ (point group $2/m$) with unit cell parameters of a = 28.8796(14) Å, b = 15.5745(6) Å, c = 12.1945(6) Å, β = 91.236°, V = 5483.6(4) $Å^3$, Z = 8. The relationship with the HTP cell parameters is: $a^{RTP} \approx 2a^{HTP}$, $b^{RTP} \approx 2b^{HTP}$, $c^{RTP} \approx c^{HTP}$. When heated to 373 K (ITP) for the second time, [TMIm][$CuCl_4$] crystallizes in the orthorhombic space group $Pnna$ (point group, mmm) with unit cell parameters of a = 12.2483(6) Å, b = 14.5106(6) Å, c = 7.8439(4) Å, V = 1394.10(11) $Å^3$, Z = 4. Entering the high-temperature phase again, [TMIm][$CuCl_4$] still crystallizes in the $C2/c$ space group, and the unit cell parameters are consistent with the previous HTP. This exactly matches with the results of the DSC test.

In RTP, as shown in Figs. 2a and d, the asymmetric unit of [TMIm][$CuCl_4$] contains two independent [TMIm] cations, one complete [$Cu1Cl_4$] anion, half [$Cu2Cl_4$] anion and half [$Cu3Cl_4$] anion. Both organic and inorganic components are in crystallographic order. Cu1, Cu2, and Cu3 atoms in special symmetry positions are penetrated by 2-fold axes parallel to the b-axis, respectively. The central copper ion and four chloride ions coordinate to form an irregular tetrahedral [$CuCl_4$] anion. The unequal Cl-Cu bond distances in [$Cu1Cl_4$] are distributed between 2.235(3) Å and 2.254(3) Å. Six groups of independent Cl-Cu-Cl bond angles range from 96.64° to 137.64° (Table S1). The unequal Cl-Cu bond distances in [$Cu2Cl_4$] are distributed between 2.226(3) Å and 2.243(2) Å. Six groups of independent Cl-Cu2-Cl bond angles range from 100.46° to 127.98°. The unequal Cl-Cu bond distances in [$Cu3Cl_4$] are distributed between 2.245(3) Å and 2.251(3) Å. Six groups of independent Cl-Cu3-Cl bond angles range from 97.20° to 133.75° (Table S2 in Supporting information). The Cl-Cu-Cl angles in the three [$CuCl_4$] tetrahedra deviate considerably from the normal 109°, implying the distortion of the [$CuCl_4$] tetrahedra.

In the ITP, as shown in Figs. 2b and e, the asymmetric unit of [TMIm][CuCl] contains half a [TMIm] cation and half a [$CuCl_4$] anion. C1 atom of [TMIm] is in a special symmetry position, crossed by a 2-fold axis parallel to the a-axis. And Cu1 atom is also in a special symmetry position, penetrated by a 2-fold axis parallel to the c-axis. The relationship between the RTP and ITP cell parameters is: $2a^{ITP} \approx b^{RTP}$, $2b^{ITP} \approx c^{RTP}$, $c^{ITP} \approx a^{RTP}$. In contrast to RTP, [TMIm] forms a 2-fold disorder with respect to the $C2$ axis parallel to the a-axis. The two independent Cu-Cl distances of the [$CuCl_4$] tetrahedron range from 2.213(3) Å to 2.226(2) Å. The four unequal Cl-Cu1-Cl angles range from 96.67° to 134.96° (Table S2). Obviously, the Cl-Cu-Cl angles of the [CuCl] tetrahedra in ITP significantly change compared to those in RTP, indicating a change in the geometric [$CuCl_4$] tetrahedra. Therefore, the phase transition of [TMIm][CuCl4] between ITP and RTP should be attributed to a synergistic effect of [TMIm] cationic order-disorder transition and [$CuCl_4$] tetrahedral anion deformation.

In HTP, as shown in Figs. 2c and f, the asymmetric unit of [TMIm][$CuCl_4$] contains one independent [TMIm] cation and one

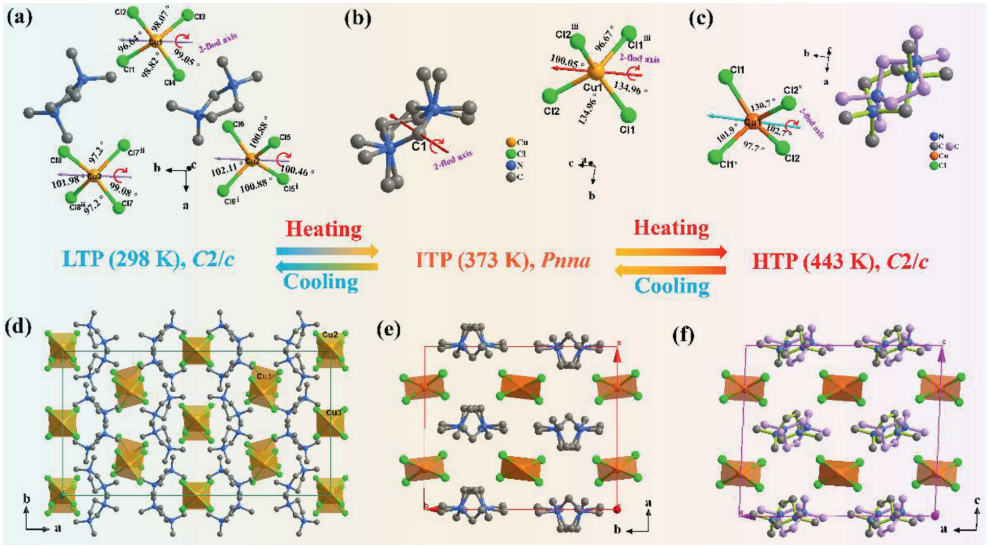

Fig. 2. The asymmetric unit of [TMIm][$CuCl_4$] at (a) 298 K, (b) 373 K and (c) 443 K, respectively. Packing view of structures of [TMIm][$CuCl_4$] at (d) 298 K, (e) 373 K and (f) 323 K, respectively. Parts of hydrogen atoms were omitted for clarity. Symmetric code: (i) 2-X, +Y, 3/2-Z; (ii) 2-X, +Y, 1/2-Z; (iii) 1/2-X, 1-Y, +Z; (v) 1-X, +Y, 3/2-Z.

half [$CuCl_4$] anion. The [$CuCl_4$] anion is located in a special symmetrical position. The Cu1 of [$CuCl_4$] is crossed by a double axis parallel to the *b*-axis. The relationship between the HTP and ITP cell parameters is: $a^{HTP} \approx c^{ITP}$, $b^{HTP} \approx a^{ITP}$, $c^{HTP} \approx b^{ITP}$. The [TMIm] cation is more dissordered than that in ITP, and the skeleton of [TMIm] cation is reversed to occupy two positions, with an occupancy rate of 0.5. The two independent Cu-Cl distances of the [$CuCl_4$] tetrahedron range from 2.197(8) Å to 2.224(6) Å. The four unequal Cl-Cu1-Cl angles range from 97.7° to 130.7° (Table S2). From ITP to HTP, there is only a small difference in the Cu-Cl distance and Cl-Cu-Cl angle. Therefore, the origin of the phase transition from ITP to HTP is mainly due to the more disordered transition of the [TMIm] cation.

In order to further explore the structural changes when the phase transition occurs, we carried out variable-temperature powder X-ray diffraction (PXRD) measurements. During both measurements, the experimental patterns of LTP, ITP and HTP are in conformity with the corresponding simulation results, indicating the phase purity (Fig. S3 in Supporting information). As shown in Fig. S2 (Supporting information), the experimental PXRD pattern remained basically unchanged when the temperature was first heated from 298 K to 373 K. When the temperature was raised to 443 K, the experimental PXRD pattern showed a significant transition, that is, several diffraction peaks vanished, while some new peaks appeared. As the temperature increased again to 343 K, the PXRD pattern also showed obvious changes. Several diffraction peaks between 18.18° and 19.54° changed, accompanied by the peaks at 25.26° and 25.26° disappearing, and the new peaks at 22.12° and 25.42° emerged. When the temperature continued to increase to 443 K, the diffraction peaks at 13.38°, 14.48°, and 22.78° disappeared, and new peaks appeared at 14.14° and 18.24°. Therefore, the diffraction peaks, which vary significantly between 298-343 K and 373-434 K, indicate the existence of two structural phase transitions in [TMIm][$CuCl_4$], which are consistent with DSC, dielectric, and crystallographic analyses.

The crystal structure analysis shows that [TMIm][$CuCl_4$] undergoes a continuous symmetric change during the heating process, namely from the *C*2/*c* space group at RTP to the *Pnna* space group at ITP, and finally to the *C*2/*c* space group at HTP. The Aizu symbol is expressed as *mmm*F2/*m*, which belongs to one of the 94 species of ferroelastic phase transitions, and thus this is a unique ferroelastic (RTP)-paraelastic (ITP)-ferroelastic (HTP) phase transition [54]. The evolution of ferroelastic domains is a distinctive feature of ferroelastic phase transitions. The ferroelastic domains of [TMIm][$CuCl_4$] were obtained by *in situ* observation of thin film samples using polarized light microscopy. As shown in Figs. 3a-e, stripe domains can be clearly observed by orthogonally polarized light at 298 K (RTP). With the rise in temperature, [TMIm][$CuCl_4$] entered the paraelastic phase (353 K, ITP), and the corresponding stripe ferroelastic domains vanished. An interesting phenomenon happens, that is, the stripe ferroelastic domains reemerged as the temperature is further increased to reach HTP, which are slightly different from those observed at ITP. Subsequently, the ferroelastic domains disappeared again when [TMIm][$CuCl_4$] returned to ITP during the continuous cooling process. After entering the RTP, the ferroelastic domains appeared again. The surface of the crystalline film did not change in heating and cooling cycle, which indicates that the evolution of ferroelastic domains depends on temperature, but not on morphology (Fig. S5 in Supporting information). The ferroelastic domains can appear and disappear repeatedly during the heating and cooling cycles, which is solid evidence that [TMIm][$CuCl_4$] undergoes a reversible ferroelastic-paraelastic-ferroelastic phase transition.

The inherent feature of ferroelastics is that there are at least two spontaneous strain orientation orders that can be switched by external stress. Therefore, we further confirm the switching of ferroelastic domains for [TMIm][$CuCl_4$] under external stress. As shown in Fig. 4a, the ferroelastic domain pattern of the as-grown

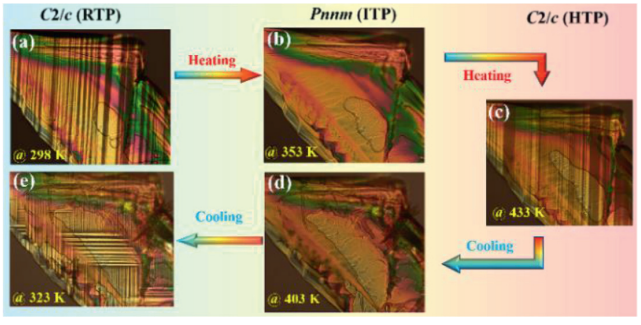

Fig. 3. (a-e) The evolution of ferroelastic domains for [TMIm][$CuCl_4$] in heating and cooling cycle.

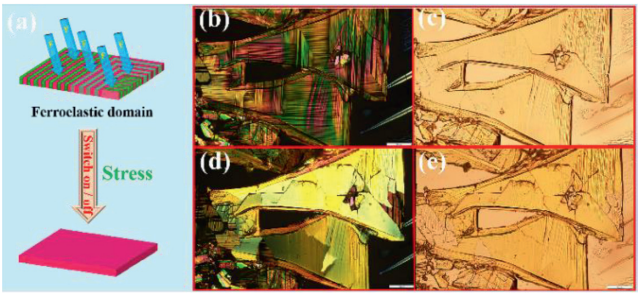

Fig. 4. (a) Schematic diagram of ferroelastic domain switching under stress. (b, d) Evolution of the ferroelastic domains in [TMIm][$CuCl_4$] under external stress stimuli observed by orthogonally polarized light microscopy. (c, e) The topography images of [TMIm][$CuCl_4$] for the corresponding region in (b) and (d), respectively.

crystalline thin films of [TMIm][$CuCl_4$] can be observed under orthogonally polarized light in RTP. After a suitable stress was applied to the surface of the crystalline film, the stripe ferroelastic domains (Fig. 4b) of [TMIm][$CuCl_4$] gradually disappeared. Finally, the ferroelastic domains tend to be monodomain or large irregular domains (Fig. 4d). From Figs. 4c and e, it can be observed that the surface of the crystalline film was not damaged after applying stress, which proved that the switching of ferroelastic domains was only related to the applied external stress, confirming the existence of ferroelasticity in [TMIm][$CuCl_4$].

Thermochromic phenomena are common in organic-inorganic Cu(II) halide systems [48,49]. The absorption band corresponding to the d-d electronic transition in the Cu^{2+} ion with the $3d^9$ electronic configuration is related to the coordination geometry of the central Cu^{2+} ion, which induces the color change of the compound [55]. The [$CuCl_4$] coordination geometry in [TMIm][$CuCl_4$] changes significantly during the phase transition from RTP to HTP, resulting in its color from yellow to reddish-brown, *e.g.*, other thermochromic organic-inorganic Cu(II) halides also exhibit phase transitions [56–58].

Due to the remarkable thermochromism of [TMIm][$CuCl_4$], solid-state UV-vis absorption spectra at different temperatures were performed. As shown in Fig. 5a, [TMIm][$CuCl_4$] appearance changed from yellow at 298 K to reddish brown at 443 K. [TMIm][$CuCl_4$] absorbs light with a wavelength less than 557 nm at room temperature, which corresponds to its yellow appearance. When the temperature was increased beyond T_{c2} to 443 K, the absorption edge moved to 597 nm, which is consistent with its reddish-brown appearance. In the UV-vis spectra of 298 K, 373 K and 443 K, the absorption edges were observed at 478, 488 and 496 nm, respectively. Furthermore, the main absorption band of the UV-vis absorption spectrum exhibits an obvious red shift with increasing temperature, revealing the color transition of [TMIm][$CuCl_4$]. On the basis of the Tauc equation, the optical band gaps were estimated to change from 2.19 eV at 298 K to 1.987 eV at 373 K (Fig. 5b). The red shift of the absorption peak and the narrowing of the band gap with the increase of temperature confirm the thermochromic phenomenon, and the change of the Cu(II) ions coordination environment during the phase transition also plays an important role in thermochromism.

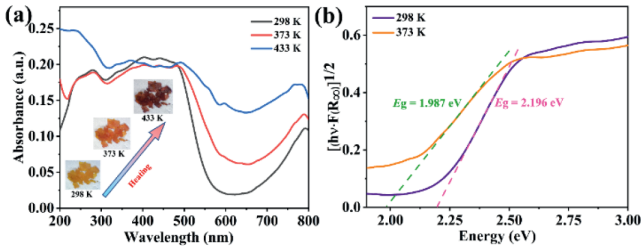

Fig. 5. (a) Variable-temperature solid-state UV-vis absorption spectra are recorded at 298 K, 373 K and 433 K. (b) The extrapolated optical band gaps for 298 K and 373 K.

In summary, [TMIm][$CuCl_4$] is an organic-inorganic hybrid ferroelastic which exhibits bistability with multi-channel physical channels (dielectric, thermochromic, and ferroelastic). Thermochromism has great potential applications in devices such as visual thermometers, temperature sensors, and information encryption. Noteworthily, a rare evolution of ferroelastic-paraelastic-ferroelastic phase occurs accompanying by the phase transition process. The ferroelastic domains of [TMIm][$CuCl_4$] can be reversibly switched not only under thermal stimulation but also under external stress. The origin of phase transition is ascribed to the synergy of order-disorder transition of [TMIm] cations and deformation of [$CuCl_4$] tetrahedral anion. This work provides powerful inspiration for exploring new excellent multifunctional switching materials.

Declaration of competing interest

There are no conflicts to declare.

Acknowledgment

This work was supported by the National Natural Science Foundation of China (Nos. 21975114, 11904151 and 22105094).

Supplementary materials

Supplementary material associated with this article can be found, in the online version, at doi:10.1016/j.cclet.2022.108127.

References

[1] Y. Zhang, H.Y. Ye, H.L. Cai, et al., Adv. Mater. 26 (2014) 4515–4520.
[2] X.X. Chen, X.Y. Zhang, D.X. Liu, et al., Chem. Sci. 12 (2021) 8713–8721.
[3] H.Y. Shen, L. He, P.P. Shi, et al., J. Mater. Chem. C 9 (2021) 4338–4343.
[4] S. Furukawa, J. Wu, M. Koyama, et al., Nat. Commun. 12 (2021) 768.
[5] H. Anetai, K. Sambe, T. Takeda, et al., Chem. Eur. J. 25 (2019) 11233–11239.
[6] Y.Y. He, Z. Chen, X.G. Chen, et al., Mater. Chem. Front. 6 (2022) 1292–1300.
[7] M. Szafranski, CrystEngComm 16 (2014) 6250–6256.
[8] Y. Liu, S. Han, J. Wang, et al., J. Am. Chem. Soc. 143 (2021) 2130–2137.
[9] D.Y. Fu, Z. Hou, Z. Chen, et al., Chin. Chem. Lett. 34 (2023) 107676.
[10] R.G. Xiong, S.Q. Lu, Z.X. Zhang, et al., Angew. Chem. Int. Ed. 59 (2020) 9574–9578.
[11] J.C. Scott, L.D Bozano, Adv. Mater. 19 (2007) 1452–1463.
[12] W. Fujita, K. Awaga, Science 286 (1999) 261–262.
[13] J.C. Scott, Science 315 (2007) 954–959.
[14] Y.Y. Tang, P.F. Li, W.Y. Zhang, et al., J. Am. Chem. Soc. 139 (2017) 13903–13908.
[15] H. Peng, J.C. Qi, X.J. Song, et al., Chem. Sci. 13 (2022) 4936–4943.
[16] C.R. Huang, Y. Li, Y. Xie, et al., Angew. Chem. Int. Ed. 60 (2021) 16668–16673.
[17] W.Q. Liao, B.B. Deng, Z.X. Wang, et al., Adv. Sci. 8 (2021) 2102614.
[18] B. Mukherjee, S.K. Batabyal, A.J. Pal, Adv. Mater. 19 (2007) 717–722.
[19] Y.Z. Hu, H.B. Zhang, W.K. Chong, et al., J. Phys. Chem. A 122 (2018) 6416–6423.
[20] Z. Wen, C. Li, D. Wu, et al., Nat. Mater. 12 (2013) 617–621.
[21] S.M. Liu, L. He, Y.Z. Wang, et al., Chin. Chem. Lett. 33 (2022) 1032–1036.
[22] J. Harada, T. Shimojo, H. Oyamaguchi, et al., Nat. Chem. 8 (2016) 946–952.
[23] D.Y. Fu, J.L. Xin, Y.Y. He, et al., Angew. Chem. Int. Ed. 60 (2021) 20021–20026.
[24] W. Li, Z. Wang, F. Deschler, et al., Nat. Rev. Mater. 2 (2017) 16099.
[25] S. Horiuchi, Y. Tokunaga, G. Giovannetti, et al., Nature 463 (2010) 789–792.
[26] H.Y. Zhang, H.H. Jiang, Y. Zhang, et al., Angew. Chem. Int. Ed. 61 (2022) e202200135.
[27] W. Yuan, X. Qu, Y. Lu, et al., Chin. Chem. Lett. 32 (2021) 2021–2026.
[28] Q.Q. Jia, L. Tong, M.M. Lun, et al., Cryst. Growth Des. 22 (2022) 2799–2805.
[29] C. Shi, L. Ye, Z.X. Gong, et al., J. Am. Chem. Soc. 142 (2020) 545–551.
[30] P.P. Shi, Q. Ye, Q. Li, et al., Chem. Mater. 26 (2014) 6042–6049.
[31] Y. Ai, R. Sun, W.Q. Liao, et al., Angew. Chem. Int. Ed. 61 (2022) e202206034.
[32] H.Y. Zhang, X.G. Chen, Z.X. Zhang, et al., Adv. Mater. 32 (2020) 20052.
[33] X.L. Liu, B. Wang, X.F. Huang, et al., J. Am. Chem. Soc. 143 (2021) 5779–5785.
[34] H. Peng, Y.H. Liu, X.Q. Huang, et al., Mater. Chem. Front. 5 (2021) 4756–4763.
[35] D.X. Liu, X.X. Chen, Z.M. Ye, et al., Sci. China Mater. 65 (2021) 263–267.
[36] M. Liu, Z.Y. Zhou, T.X. Nan, et al., Adv. Mater. 25 (2013) 1435–1439.
[37] K.J. Lee, B. Turedi, A. Giugni, et al., Adv. Funct. Mater. 31 (2021) 2008088.
[38] J. Wang, H. Shen, W. Li, et al., Adv. Sci. 6 (2019) 1802019.
[39] S.N. Du, D. Su, Z.Y. Ruan, et al., Angew. Chem. Int. Ed. 61 (2022) e202204700.

[40] C. Shi, J.J. Ma, J.Y. Jiang, et al., J. Am. Chem. Soc. 142 (2020) 9634–9641.
[41] X.Q. Huang, H. Zhang, F. Wang, et al., J. Phys. Chem. Lett. 12 (2021) 5221–5227.
[42] X.T. Zhou, Y. Wu, Q.X. Xie, et al., Scripta Mater. 177 (2020) 172–175.
[43] H.Y. Liu, H.Y. Zhang, X.G. Chen, et al., J. Am. Chem. Soc. 142 (2020) 15205–15218.
[44] P.P. Shi, Y.Y. Tang, P.F. Li, et al., Chem. Soc. Rev. 45 (2016) 3811–3827.
[45] Y.S. Xue, Z.X. Zhang, P.P. Shi, et al., Chin. Chem. Lett. 32 (2021) 539–542.
[46] Y.Y. Yu, P.Z. Huang, Y.Z. Wang, et al., Chin. Chem. Lett. 32 (2021) 3558–3561.
[47] Y.P. Gong, X.X. Chen, G.Z. Huang, et al., J. Mater. Chem. C 10 (2022) 5482–5488.
[48] B. Sun, X.F. Liu, X.Y. Li, et al., Angew. Chem. Int. Ed. 59 (2020) 203–208.
[49] J.C. Liu, W.Q. Liao, P.F. Li, et al., Angew. Chem. Int. Ed. 59 (2020) 3495–3499.
[50] Y.H. Liu, J.C. Liu, H. Peng, et al., CrystEngComm 23 (2021) 264–267.
[51] E.I. Kozliak, J. Chem. Educ. 84 (2007) 493–498.
[52] M.A. Asghar, J. Zhang, S. Han, et al., Chin. Chem. Lett. 29 (2018) 285–288.
[53] M.J. Yang, H. Cheng, Y.Q. Xu, et al., Chin. Chem. Lett. 33 (2022) 2143–2146.
[54] K. Aizu, J. Phys. Soc. Jpn. 27 (1969) 387–396.
[55] D. Cortecchia, H.A. Dewi, J. Yin, et al., Inorg. Chem. 55 (2016) 1044–1052.
[56] B. Huang, J.Y. Zhang, R.K. Huang, et al., Chem. Sci. 9 (2018) 7413–7418.
[57] D.R. Bloomquist, M.R. Pressprich, R.D. Willett, J. Am. Chem. Soc. 110 (1988) 7391–7398.
[58] A. Caretta, R. Miranti, A.H. Arkenbout, et al., J. Phys. Condens. Mat. 25 (2013) 505901.